Processing Bulk Nanostructured Materials

Effect of pre-annealing on the formation of the ω-phase in the Ti-2 wt%V alloy after high-pressure torsion

G. S. Davdian[1,2], A. S. Gornakova[1], B. B. Straumal[1,2,*], A. Korneva[3], N. S. Afonikova[1], E. A. Novikova[2], and A. I. Tyurin[4]

[1] *Osipyan Institute of Solid State Physics of the Russian Academy of Sciences, Ac. Osipyan Str. 2, Chernogolovka, Russia 142432*

[2] *Department of Physical Chemistry, National University of Science and Technology MISiS, Leninskiy Ave. 4, Moscow, Russia 119049*

[3] *Institute of Metallurgy and Materials Science, Polish Academy of Sciences, Reymonta St. 25, 30-059 Cracow, Poland*

[4] *Institute "Nanotechnology and Nanomaterials", G.R. Derzhavin Tambov State University, Internatsionalnaya Str. 33, Tambov, Russia 392000*

ABSTRACT

Although vanadium is used in many alloys as an alloying element, the binary Ti–V system has been studied very poorly. In particular, the effect of heat treatment in combination with high-pressure torsion (HPT) has not been studied at all for this system. The Ti-2 wt%V alloy was pre-annealed at three temperatures in two different regions of the Ti–V phase diagram, namely at 400 °C (α phase), 700 °C (α phase) and 1000 °C (β phase). The as-cast state was also investigated. After annealing and quenching, all four samples contained only the α/α' phase. After the HPT, the ω-phase appeared in the material. Its portion increased from 70 to 76% with an increase in the pre-annealing temperature, but the as-cast sample had after HPT the largest proportion of ωTi phase of 86%. The values of nanohardness (H) and Young's modulus (E) after HPT were measured. H increased from 5.1 ± 0.1 to 6.4 ± 0.1 GPa with increasing pre-annealing temperature. The steady-state value of torsion torque during HPT also increases from 1533 to 2094 N m. However, the E value remained almost unchanged at 147 ± 3 GPa. The microhardness of the samples after HPT increased by about two times compared to the annealed samples.

🍷 Springer

Introduction

The titanium alloys possess the combination of low density (4500 kg/m^3), excellent mechanical properties (strength ~ 1000 MPa, ductility ~ 10%) and good corrosion resistance. Therefore, they belong to the best engineering materials [1]. The structure and properties of titanium alloys can be tailored by alloying combined with thermal and mechanical treatments [2]. The thermal and mechanical treatments are especially productive since titanium has different allotropic modifications at low (α-phase) and high (β-phase) temperatures. Titanium possesses also an ω-phase which is stable at high pressure. It is generally believed that the transitions of α-Ti and β-Ti to ω-phase (reversible α-to-ω and β-to-ω transformations) can be used to improve the mechanical properties of the Ti-based alloys. It is very important to know the peculiarities of the ω phase formation and its stability at high temperatures in order to be able to plan the targeted thermomechanical treatment of the Ti alloys.

The equilibrium phase diagram for pure titanium in the "temperature–pressure" coordinates can be found for example in Ref. [3]. In pure Ti, the transition from αTi to ωTi phase proceeds at high-pressure [4–12]. The α-ω-β triple point in titanium was observed in experiments at 7.5 GPa and 640 °C [10]. The α-phase transforms into ω one at ambient temperature between 2.9 and 10.5 GPa. The α-to-ω transition pressure depends on the conditions of experiments, on the sample structure and on the pressure environment [8–12].

The low-temperature allotropic modification α-Ti possesses the hexagonal close packed (hcp) crystal structure (space group P63/mmc, Wyckoff's positions 2c). Its ratio of the lattice parameters is $c/a \approx 1.58$. Above 882 °C, the body-centered cubic (bcc) β-Ti allotropic modification is stable. It possesses the space group Im3m. The Ti atoms occupy in this lattice the 2a Wyckoff's positions. The crystal structure of the high-pressure allotropic modification ω-Ti is hexagonal (space group P6/mmm). The Ti atoms occupy in the ω-phase the 1a and 2d Wyckoff's positions [8, 13]. In Refs [8, 13], the mechanism of the α-to-ω (or α-to-β-to-ω) crystallographic phase transformations was analyzed. The authors of [8, 13] suggested that at low temperatures, the α-to-ω phase transformation proceeds as a α-to-β-to-ω transitions sequence. It means that the α-phase transforms first into β-phase and then to ω-phase. We remember here that β-phase is thermodynamically unstable below 882 °C in the undoped

Ti [8]. The α-to-ω (or α-to-β-to-ω) transformations are of martensitic-type. Such transformation is characterized by a rather large hysteresis. It means that after pressure release, the ω-phase can be retained in the material [6]. In certain Ti-based alloys, the metastable ω-phase can be produced even without high pressure, just by using a certain heat treatment [5, 7].

However, in the transformations of binary Ti-based alloys, not only α, β and ω phases are involved [14]. Thus, if the concentration of atoms stabilizing β-Ti phase in binary Ti alloys is low, the hexagonal closely packed (hcp) α' martensite (space group P63/mmc) or the orthorhombic α'' martensite (space group Cmcm) [15] can be created from the body-centered cubic (bcc) β-phase at high cooling rate [16–20]. In most cases, the α' martensite appears at lower concentrations of alloying elements, and the α'' martensite forms at higher contents of β-stabilizers [21, 22]. The appearance of α' and α'' martensites in the Ti alloys strongly influences their microstructure and properties [16–20].

Severe plastic deformation (SPD) by the high-pressure torsion (HPT) permits to obtain the extremely fine-grained structure in Ti and Ti alloys [23–29]. They can contain also the metastable ω-phase which remains in the alloys after high pressure release. And even more, the SPD permits to drastically enhance the mechanical properties of titanium and Ti-based alloys [30, 31]. For example, the unique combination of high strength and ductility was achieved in nanograined titanium [30, 31]. The ω-phase can appear after SPD also in zirconium, but it was not observed after HPT in hafnium [32, 33].

In small concentrations, the alloying titanium with vanadium improves its strength and plasticity. Therefore, the addition of vanadium is widely used in titanium alloys. Vanadium has a similar crystal structure to β-Ti, a similar electronic structure, and an almost equal atomic size. This leads to unlimited solubility of vanadium in β-Ti and limited in α-Ti (1–3 wt% at 700 °C), and also reduces the temperature of $\alpha \rightarrow \beta$ allotropic transformation. If the vanadium content in the alloy does not exceed 8–10 wt%, the $\beta \rightarrow \alpha'$ or $\beta \rightarrow \alpha''$ martensitic transformation occurs during quick quenching from the β region. An increase in the concentration of vanadium in α' Ti–V alloys increases their hardness and strength, whereas for α'' Ti–V alloys, the strength and hardness decrease with increasing V content. The plasticity of Ti–V alloys varies inversely [34–36]. The first studies of this binary system showed the existence of a monotectoid reaction $\beta \rightarrow \alpha$Ti + V on

the diagram. At 675 °C, the αTi + V mixture transforms by cooling into $\alpha + \beta$ one by a monotectoid reaction [37]. However, more recent studies have shown that such a reaction is possible only in the presence of a sufficient amount of oxygen, whereas in oxygen-free Ti–V alloys, the αTi + V region and monotectoid reaction are absent [38, 39]. To date, studies have been conducted on the effect of pre-annealing temperature and high-pressure torsion (HPT) of binary titanium alloys like Ti–Nb [40–42], Ti–Fe [43–46], Ti–Mo [47–49] and several others, even such unusual as Ti–Pt [50]. The authors of the research on Ti-3 wt%Nb [42] and Ti-2–4.5 wt%Fe [44] alloys found the dominant fraction of the α phase after annealing. Its content was 85% or more. In both cases, the annealed samples were subjected to HPT with the same parameters. After HPT, the samples have high amount of ω phase (> 75%). Vanadium is often used as an alloying element in titanium-based alloys, but the effect of HPT on binary titanium–vanadium alloys has not been studied yet. Therefore, the purpose of this work is to study the effect of the pre-annealing temperature on the structure and properties of vanadium-doped titanium treated with high-pressure torsion.

Experimental and methods

The binary Ti-2 wt%V alloy has been produced from pure components (99.98 wt% Ti and 99.98 wt% V) using the levitation method in vacuum. In this method, the molten metal "levitates" in a cold crucible, which is a set of vertically standing water-cooled copper pipes. Around the crucible, a water-cooled copper induction coil is placed. The water-cooled copper induction coil excites in the crucible a powerful magnetic field of supersonic frequency. Foucault eddy currents are induced in the molten metal, causing intense heating of the metal up to its melting point. At the same time, eddy currents create an opposite magnetic field around the melt, which interacts with the primary field and generates Lorentz forces. The Lorentz forces allow the liquid–metal bath to float in a vacuum or inert atmosphere without touching the walls of the cold crucible. The approximate heating temperature of the alloy during levitation is 1700 °C (melting point of Ti-2 wt%V alloy is about 1665 ± 3 °C), and the levitation time is approximately 10–15 s. As a result, a cylindrical ingot with a diameter of 10 mm

was obtained from which 0.7-mm-thick disks were cut using an electroerosive machine.

After that, the samples were sealed in quartz ampoules and annealed in vacuum at a residual pressure of 4×10^{-4} Pa. Samples of a binary Ti-2 wt%V alloy were examined with pre-annealing temperatures: 400 °C for 1992 h, 700 °C for 1896 h. and 1000 °C for 24 h. The annealing temperatures were in the α and β areas of the Ti–V diagram, respectively [38].The pre-annealing time was chosen in such a way that it could be sufficient to achieve a homogeneous state of the samples. Figure 1 shows the phase diagram of the Ti–V alloys with red points which are showing the pre-annealing conditions.

After annealing, the samples were quenched by immersing ampoules with samples in water. The HPT was carried out using a custom-made computer-controlled device manufactured by W. Klement GmbH (Lang, Austria). The annealed samples were HPT-processed at room temperature, pressure of 7 GPa, deformation rate of 1 rpm and 5 revolutions of the plunger. The samples obtained as a result of HPT changed in thickness by 2 times, from 0.7 to 0.35 mm. Structural-phase analysis was carried out using a Rigaku SmartLab X-ray diffractometer (Rigaku, Tokyo, Japan) in Cu–K$_{\alpha1+\alpha2}$ radiation, wavelength 0.15419 nm. Phase analysis and calculation of lattice parameters were carried out using the PowderCell 2.4 program (PowderCell for Windows Version 2.4. 03/08/2000, Werner Kraus & Gert Nolze, BAM, Berlin, Germany). The micrographs with the scanning electron microscope (SEM) were taken on the Axia ChemiSEM HiVac device (Thermo Fisher Scientific, Brno, Czech Republic). To qualitatively determine the presence of oxygen in the samples,
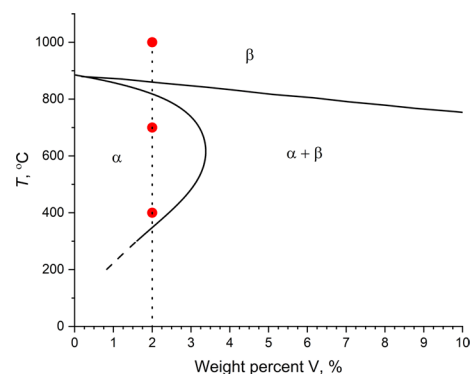

**Figure 1** Phase diagram of the Ti–V system. Red points show the pre-annealing conditions [38].

a wave spectrometer with low efficiency but high sensitivity was used. INCA software allows simultaneous operation of ED (energy dispersive) and WD (wavelength dispersion) spectrometers (mode Energy +) to take into account all the details of overlapping individual lines of characteristic X-ray radiation (Tescan Vega TS5130 MM Oxford Instruments, Ulm, Germany). The oxygen content in our samples is about 2 wt%. Transmission electron microscopy (TEM) was performed using the JEM-2100 instrument (JEOL Ltd, Akishima, Japan). Nanohardness measurements were carried out on a nanotester Triboindenter TI-950 (Hysitron, Eden Prairie, Minnesota USA) device equipped with a Berkovich indenter (Bruker, Billerica, Massachusetts, USA). Measurements were carried out along the diameter of the samples; the loading rate was constant and equal to $dP/dt = 40$ mN/s. The maximum load was $P_{max} = 10$ mN. Before the measurements, the surface of the samples was polished on a diamond paste with grain size of 1 μm. The values of nanohardness (H) and Young's modulus (E) were determined by the Oliver-Farr method based on characteristic P–h diagrams [51–53]. The average values of H and E are obtained by averaging the obtained results. Nanohardness measurements are considered to be measurements of the surface properties of a material; therefore, to measure the volumetric properties,

we additionally measured the microhardness of the samples. The microhardness of the alloy was measured using an ITB-1 IMC hardness tester (Metrovest LLC, Neftekamsk, Russia). At a load of 200 g, the exposure time is 15 s, 10 measurements per point. On the samples after HPT treatment, measurements were carried out in the middle of their radii.

Results

In Fig. 2, the SEM and light micrographs of the Ti-2 wt%V alloy (a) as-cast and after annealing at (b) 400 °C, (c) 700 °C, (d) 1000 °C and quenching are shown. The martensitic plates are clearly visible in Fig. 2d. The microstructures in Fig. 2a, b, d more resemble the lamellar ones. The structures of Fig. 2a, b, d, after different heat treatment, do not differ significantly from each other. The absence of differences in the structures of the as-cast sample and the annealed one in the βTi-phase region can be explained quite simply. Namely, after melting, the sample undergoes the βTi → αTi → αTi + βTi path during cooling. It means that during the quenching process, a βTi-phase is formed from the melt in the material at the beginning, which, upon further cooling, begins to turn into an αTi-phase. Then, due to the hardening and the mechanism of martensitic transformation, the part of the βTi-phase passes and remains in the

Figure 2 SEM and optical microscope micrographs of the Ti-2 wt%V alloy **a** as-cast and after annealing at **b** 400 °C, **c** 700 °C, **d** 1000 °C, and quenching.
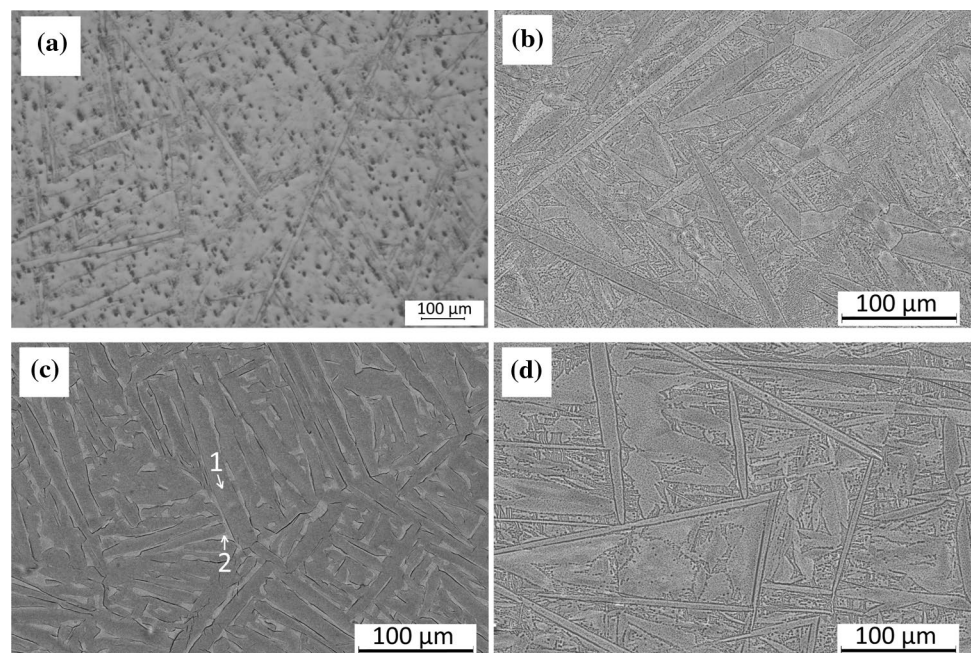
form of martensite. For a sample annealed at 1000 °C, however, the transition to the βTi-phase occurs during annealing, and not during cooling from the melt. Then, the question remains with the sample annealed at 400 °C. The data on the diffusion coefficient of vanadium in titanium differ greatly in different references, sometimes by a couple of orders of magnitude. Nevertheless, all of them indicate an extremely low diffusion coefficient of vanadium in titanium. The recalculation showed that at the selected temperature (400 °C) and time (1996 h), vanadium practically does not diffuse in the alloy. It means that the structure shown in Fig. 2b should be similar to that in Fig. 2a, which corresponds to our results. It should be emphasized that the boundaries of the matrix grains in these structures are implicit, and the discussion is about the internal structure of the matrix grains. The microstructure of as-cast sample, as well as of sample annealed at 400 °C and at 1000 °C, have martensitic needle plates of αTi-phase with a thickness of 8 ± 3 μm, with many globular grain phases of various sizes. The structure of the sample annealed at 700 °C, Fig. 2c, has a pronounced lamellar structure, with the lamellae containing about 1.6% V solved. Also they are wetted by a lighter phase containing 6.4% V. XRD did not show the presence of a second phase, and the maximum solubility of V in the αTi-phase is about 3.7 wt% V. The question of what wets the αTi-phase lamellae requires a more detailed study, which is not important for this work.

X-ray diffraction (XRD) analysis was performed on the studied samples before and after the HPT (Fig. 3). Some peaks on the XRD patterns are marked as $(\alpha + \omega)$ or $(\beta + \omega)$. This is due to the superposition of two peaks from different phases. In addition, it is important to note that after HPT the peaks become wide (black lines) due to the grain refinement and texturing of samples. The peaks after annealing (red lines) have mainly the peaks of the α-phase, even after annealing in the β phase region (1000 °C) and subsequent quenching. After HPT, peaks of the ω phase appeared, and an additional peak of the β phase also appeared in the sample pre-annealed at 1000 °C.

In the samples annealed at 400 and 700 °C, the αTi peaks corresponding to the planes disappeared after the HPT: (2, 0, 0), (1, 1, 2), (2, 0, 1), (0, 0, 4), (2, 0, 2), (1, 0, 4), (2, 0, 3) and (2, 1, 0). In the sample annealed at 1000 °C, in addition to the listed ones, disappear also (1, 0, 2), (2, 1, 1), (2, 1, 2) peaks. In other words, HPT leads to the disappearance of the αTi peaks, and the formation of ωTi and βTi phases.

Table 1 contains the values for portions of α/α' and β-phases and their lattice parameters in the Ti-2 wt%V as-cast and annealed samples. In all annealed samples, the main phase after quenching is α/α'-Ti. The average grain size in the αTi phase is 40 ± 10 nm and in the βTi phase is 65 ± 5 nm. The estimation of the average grain size of the phases, which we associate with the size of the coherent scattering regions, was carried out using the PowderCell 2.4 program, which uses the full-profile Rietveld method.

After HPT, the main phase in the samples becomes the ωTi phase, and the βTi phase is absent in samples as-cast and pre-annealed at 400 and 700 °C. It appears in sample pre-annealed at 1000 °C. The portion of the ωTi phase increases with an increase in the pre-annealing temperature from 70 to 76% (Table 2). However, the as-cast alloy has the largest proportion of ωTi phase of 86%.

The lattice parameter a in the α/α'-Ti decreases after HPT (Fig. 4a) and the lattice parameter c increases (Fig. 4b). It means that the c/a value in the α/α'-Ti phase increases after HPT (Fig. 4c).

The microstructure of alloys after HPT treatment was investigated using TEM (Fig. 5). For the studied images, bright-field (Fig. 5a, d, g) and dark-field (Fig. 5b, e, i) images were made, the average grain size was estimated in the dark-field images. The difficulty of estimating the average grain size was the presence of a large number of grain conglomerates. Processing of dark-field images showed that the average grain size is 75 ± 5 nm. SAED diagrams taken from the entire area of Fig. 5a, d showed the presence of two main α and ωTi phases.

During the processing of HPT samples, the torsion torque was measured depending on the angle of rotation (Fig. 6a). An increase in the pre-annealing temperature increases the torque value. Thus, already at the initial stage of the HPT, the torque increases from 1533 N m in the sample pre-annealed at 400 °C, to 1927 N m after pre-annealing at 700 °C and to 2094 N m after pre-annealing at 1000 °C. Figure 6b shows the dependence of the applied load P on the indentation depth h for HPT treated samples. The P–h dependences were measured in the middle of the radius of the samples. There is clearly a correlation between the dependence of the torque on the rotation angle at saturation and the dependence of the indentation depth on the load. It means that with the same applied load, the sample is pressed deeper, which reaches saturation at lower torque values. For
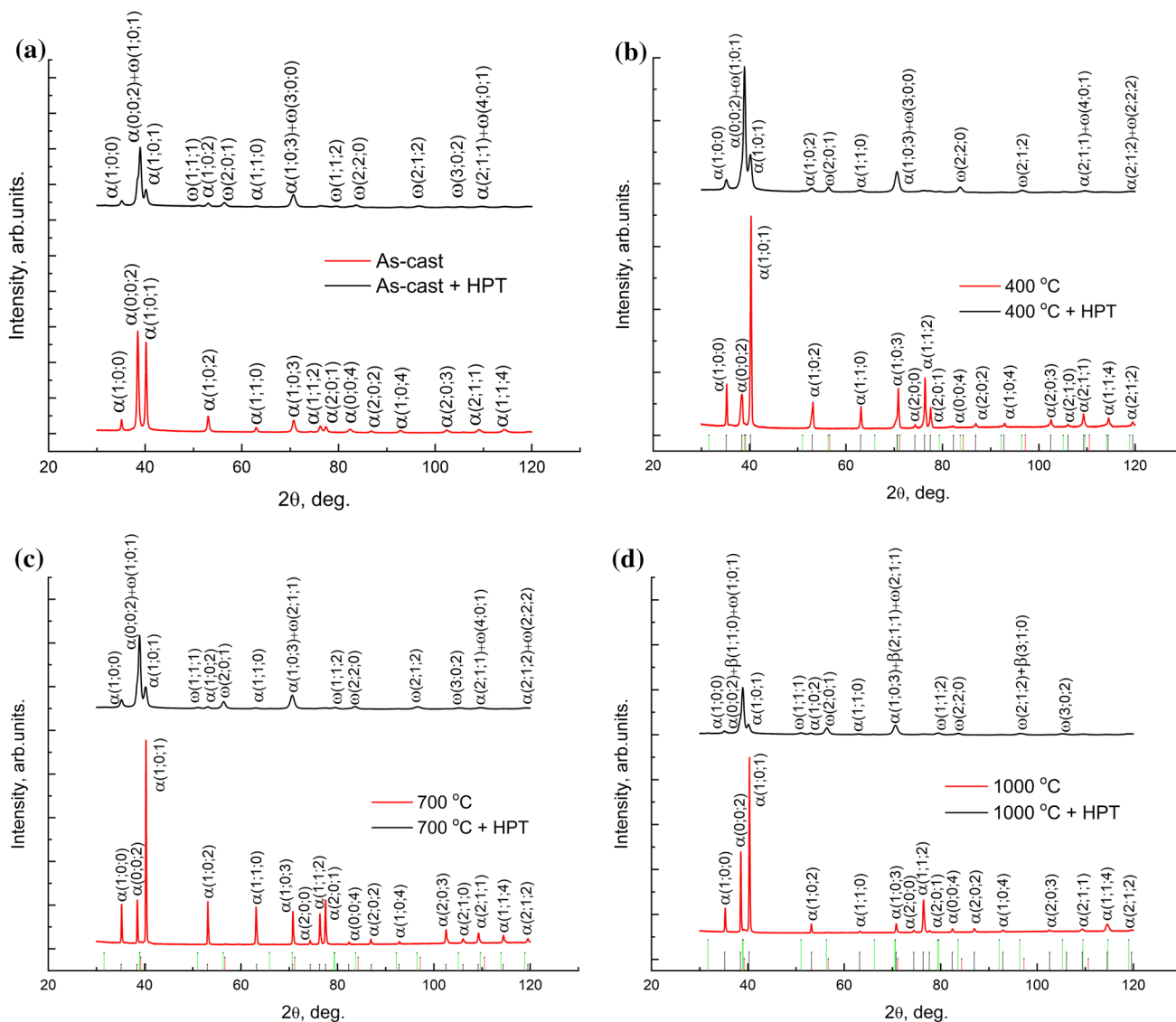
Figure 3 XRD patterns of the Ti-2 wt%V alloy **a** as-cast and annealed at **b** 400 °C, **c** 700 °C, **d** 1000 °C, before (red lines) and after HPT (black lines).

Table 1 Portions of α- and β-phases *V* and their lattice parameters *a* and *c* in Ti-2 wt%V alloy after annealing

T, °C	α/α'		β	
	V, %	*a, c*, nm	*V, %*	*a*, nm
as-cast	100	0.2948(1); 0.4678(1)	–	–
400	99 ± 1	0.2946(1); 0.4684(1)	1 ± 0.5	0.3246(1)
700	99 ± 1	0.2948(1); 0.4684(1)	1 ± 0.5	0.3246(1)
1000	99 ± 1	0.2944(1); 0.4680(1)	1 ± 0.5	0.3246(1)

example, at a load of 8 mN, the indenter is pressed into pre-annealed samples at 400, 700 and 1000 °C to a depth of 269.9, 220.6 and 218.4 μm, respectively, while

their saturation output is at 1530, 1930 and 2070 N m, respectively.

In our case, the pre-annealing of the Ti-2 wt%V alloy significantly affected its mechanical characteristics, such as steady-state torsion torque, hardness and strength.

Based on the measurement results for nanohardness (*H*) and Young's modulus (*E*), two types of graphs were compiled: the first shows the dependence of the *H* and *E* values on the measurement location on the disk, determined by its distance from the center (Fig. 7a, c). The second shows the average values depending on the annealing temperature

Table 2 Portions of α, β, ω-phases V and their lattice parameters a and c in Ti-2 wt%V alloy after HPT

T, C+HPT	α/α'		β		ω	
	V, %	a, c, nm	V, %	a, nm	V, %	c, a, nm
as-cast	14 ± 1	0.2950(1); 0.4676(1)	–	–	86	0.4624(1)
400	30 ± 1	0.2945(1); 0.4691(1)	–	–	70 ± 1	0.4626(1); 0.2823(1)
700	27 ± 1	0.2946(1); 0.4685(1)	–	–	73 ± 1	0.4624(1); 0.2829(1)
1000	15 ± 1	0.2945(1); 0.4686(1)	9 ± 1	0.3248(3)	76 ± 1	0.4624(1); 0.2819(1)
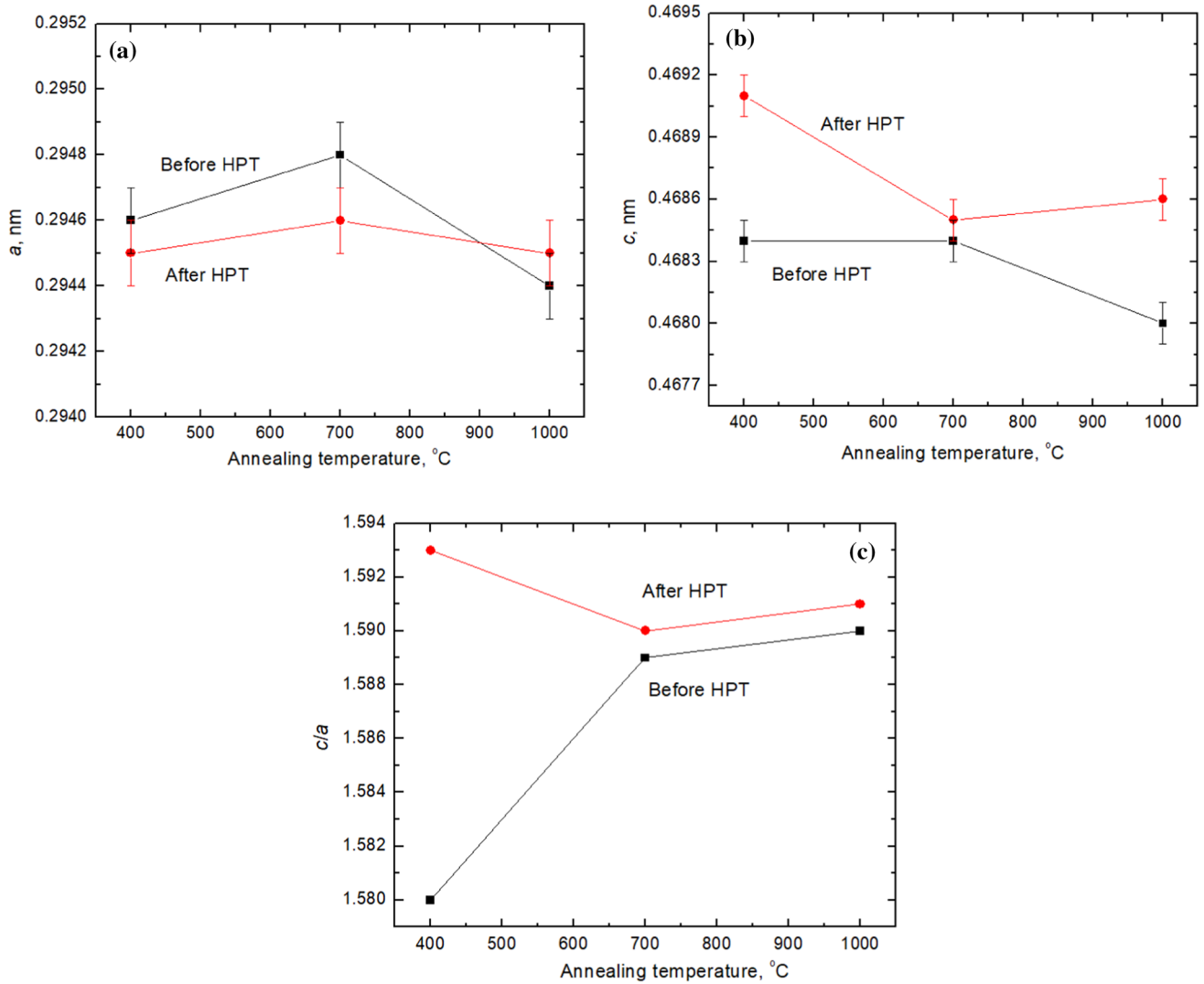
Figure 4 Dependence of the lattice parameters in the α/α' phase on the annealing temperature before and after HPT. **a** Lattice parameter a. **b** Lattice parameter c. **c** Relationship c/a

(Fig. 7b, d). The averaging took place over the entire sample. Due to the large variation in the hardness values of the sample pre-annealed at 400 °C, its error is significantly higher than that of other samples.

Figure 7a clearly shows the lack of uniformity of nanohardness in the sample annealed at 400 °C. The minimum around 4.5 ± 0.1 GPa appears in the center of the sample. At the same time, samples annealed
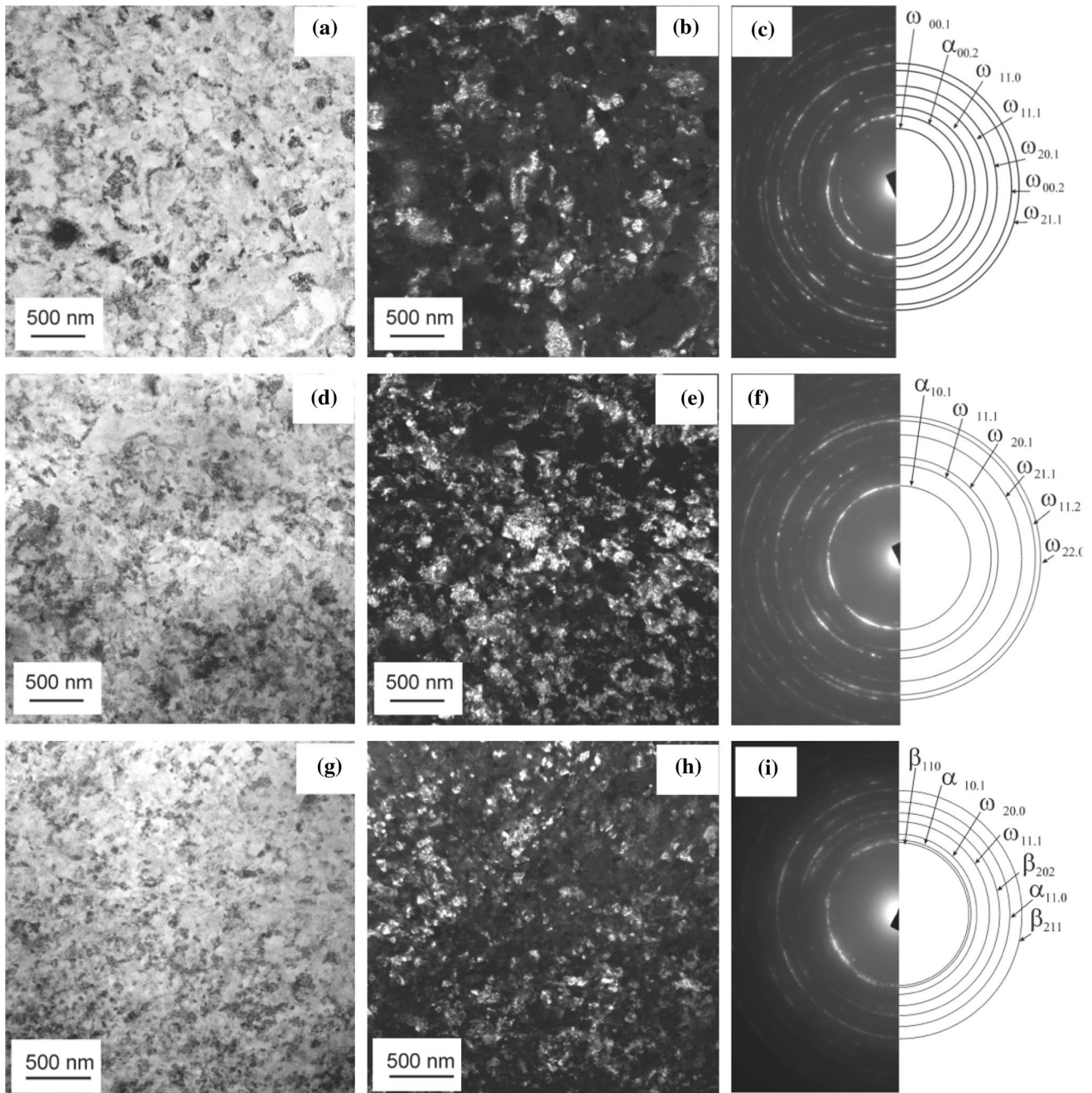
Figure 5 TEM micrographs of the Ti–2 wt%V alloy after HPT deformation and pre-annealing at 400 °C (**a–c**), 700 °C (**d–f**) and 1000 °C (**g, h**). Bright field (**a, d, g**), dark-field (**b, e, i**) images, as well as SAED patterns (**c, f, h**)

at 700 and 1000 °C are uniform. It can be concluded from this fact that the parameters of pre-annealing effect the uniformity of properties in the samples after HPT. In addition, Fig. 7b shows that an increase in the annealing temperature leads to an increase in the average values of nanohardness.

Additionally, microhardness measurements were carried out, which confirmed the decrease in hardness of the sample that underwent heat treatment at 400 °C (Fig. 7e). Figure 7f shows the values of microhardness of as-cast, annealed and after HPT
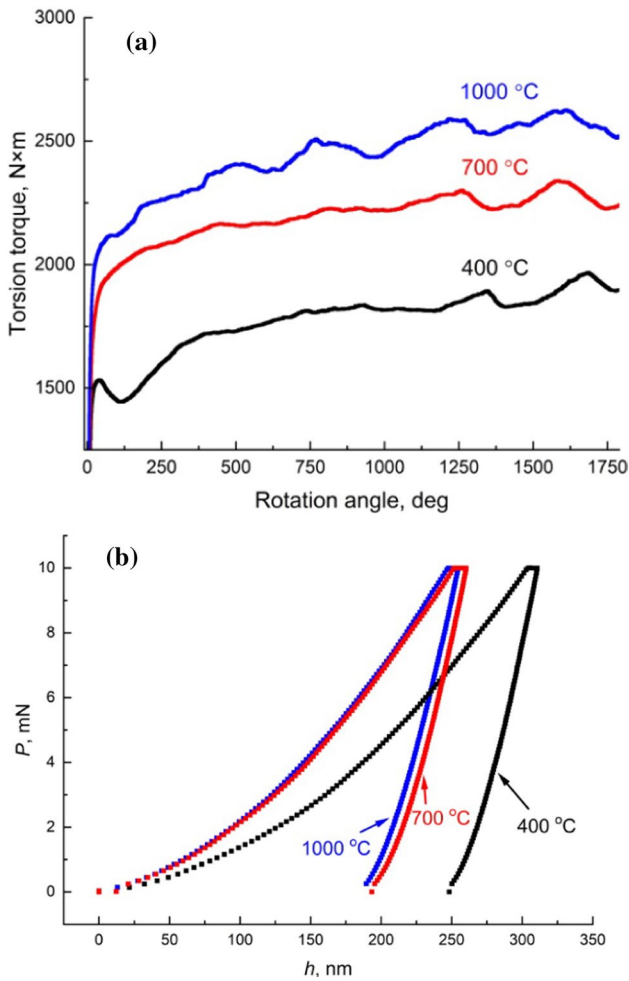
Figure 6 **a** Dependences of torsion torque on the rotation angle for the Ti-2 wt%V alloy pre-annealed at 400 °C (black line), 700 °C (red line), 1000 °C (blue line). **b** Dependence of the applied load P on the depth h of indentation for the same samples after HPT

processing samples. The hardness of the samples after HPT processing has more than doubled.

Discussion

In Ref. [14], the as-cast Ti–Fe alloys were annealed in the β-(Ti,Fe) solid solution region and then quenched. As a result, at low Fe content < 2 wt% Fe, the β-(Ti,Fe) solid solution transformed into α'-Ti martensite. During following HPT, the α'-Ti martensite partly transformed into ω-Ti. However, the a and c lattice parameters of remaining portion of α'-Ti phase increased. Thus, a and c shifted toward the a and c values for

iron-free pure α-Ti. These processes included an increased mass transfer of iron atoms out of α'-Ti. Here, we observed that in the Ti–2 wt%V alloy, the lattice parameters a and c change after HPT in different directions. Namely the a value in the α/α'-Ti decreases after HPT (Fig. 4a), and the lattice parameter c increases (Fig. 4b). It means that the c/a value in the α/α'-Ti phase increases after HPT (Fig. 4c).

The important result of HPT of studied Ti–2 wt%V alloy is the formation of ω-phase. Its amount after HPT (see Table 2) is about 70%, and it increases from 70 ± 1 to $76 \pm 1\%$ with increasing temperature of pre-annealing (from 400 to 1000 °C). From this point of view, the Ti–2 wt%V alloy is similar to the previously studied Ti–Fe [14, 54], Ti–Co [55], Ti–Mo [56] and Ti–Nb [57] alloys. Moreover, the rather high amount of ω-phase in this work is comparable to the situation when the pre-annealed Ti-based alloys contained the β-phase or the mixture of α- and β-phases. It was observed that a special orientation relation exists between β- and ω-phases which makes easy the martensitic β-to-ω transition. For example, the alloying of titanium with iron allows one to precisely fit the lattice periods of β- and ω-phases in such a way that the amount of ω-phase after HPT can reach almost 100% [54]. If we substitute the 4 wt% Fe in the alloy with 4 wt%Co, the amount of ω-phase after HPT immediately drops down because the β and ω lattices with Co instead of Fe do not so ideally fit each other [14].

If the β-phase is present in the sample, it can help to transform the α-phase into ω-phase during HPT [54]. To the contrary, if the sample was pre-annealed below the temperature of eutectoid transformation of β-phase into the mixture of α-phase and intermetallic compound, the direct α-to-ω transformation is quite sluggish. It is because the orientation relationship for the martensitic α-to-ω transformation is not so favorable as for the β-to-ω one. For example, in the Ti–4 wt% Fe and Ti–4 wt% Co alloys pre-annealed in the $\alpha + \beta$ area of the respective phase diagram, the portion of ω-phase after HPT is much higher than in the case when the same alloys were pre-annealed in the α + TiFe or α + Ti$_2$Co areas [14]. Moreover, the increase in cobalt content in the α-Ti-based solid solution drastically diminished the portion of ω-phase after HPT. It decreased from 80% in the Ti–4 wt% Co alloy pre-annealed at 400 °C to zero in the samples annealed above 600 °C [14].

Today, SPD is a widely studied way to improve the properties of metallic alloys. During SPD, various
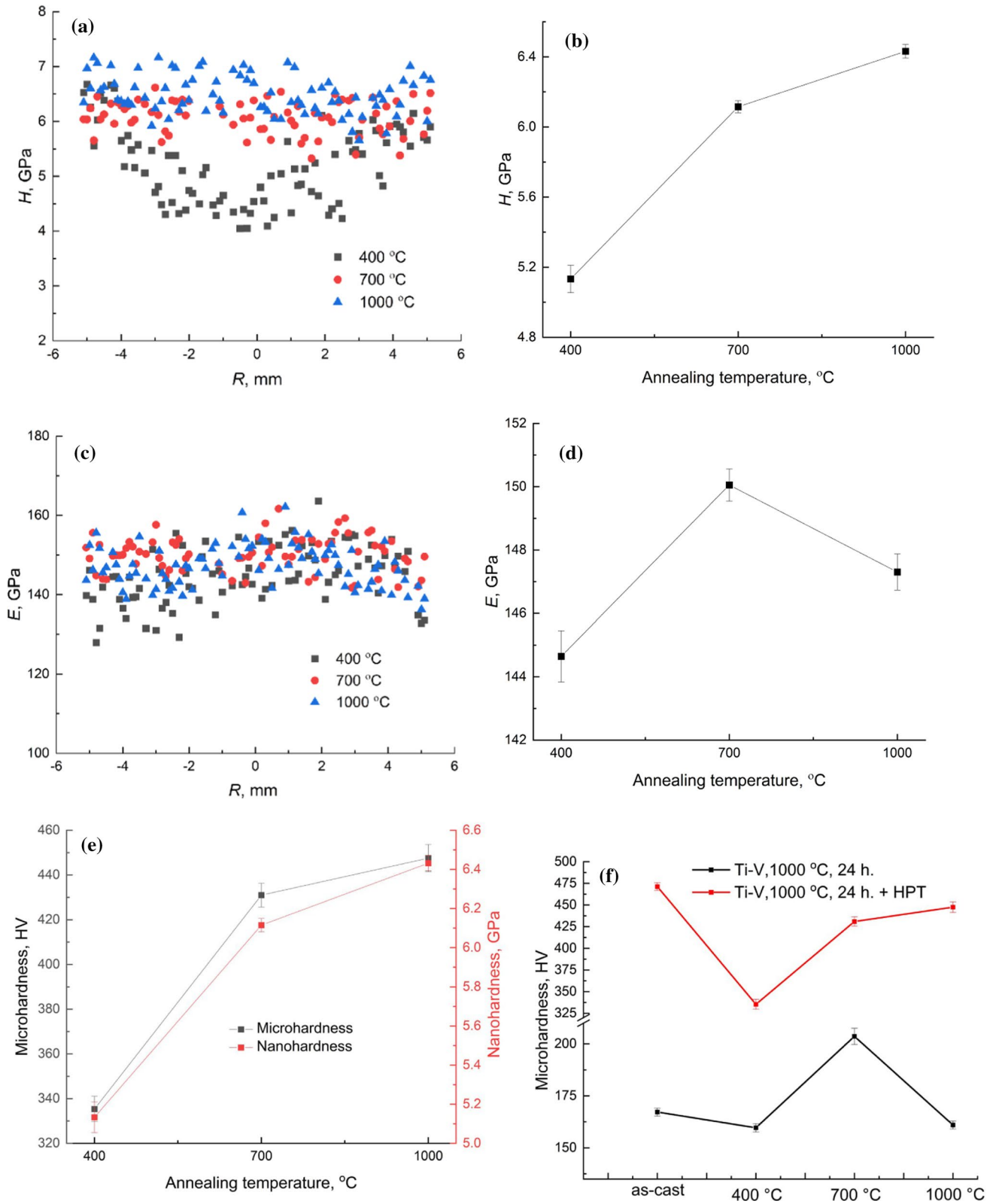
◀**Figure 7** **a** Nanohardness values (*H*) measured after HPT along the diameter of the Ti-2 wt%V alloy samples pre-annealed at 400 °C (black squares), 700 °C (red circles), 1000 °C (blue triangles). **b** The dependence of averaged *H* values on the pre-annealing temperature. **c** The values of Young's modulus (*E*) determined after HPT along the diameter of the Ti-2 wt%V alloy samples pre-annealed at 400 °C (black squares), 700 °C (red circles), 1000 °C (blue triangles). **d** The dependence of averaged *E* values on the pre-annealing temperature. **e** Dependences of microhardness and nanohardness on the pre-annealing temperature. **f** Dependences of microhardness for annealed and after HPT samples

lattice defects are formed, grain size decreases, and phase transformations occur. All this changes the properties of the treated alloy. High-pressure torsion is one of the important modes of severe plastic deformation [58–61]. In all studies of titanium-based alloys where hardness was measured, it increased after SPD, sometimes by two times or more [29, 39–50, 62–64].

In our studies, the analysis of the phase composition of annealed samples for all annealing temperatures showed a small amount of the β-phase of about 0.5–1 wt%. In the Ti-3 wt% Nb alloy, the portion of the β-phase was about 10% [10], and in Ti-Fe alloys, the portion of the β-phase varied from 0 to 15% [45]. In cases when β-phase was absent, the 3–8% of TiFe intermetallic was present [45]. In this work, the HPT of Ti-2 wt%V alloy led to the formation of 70–76% of the ω-phase. Moreover, the increase in the pre-annealing temperature also led to an increase in the portion of the ω-phase after HPT. A similar HPT treatment for Ti-Nb and Ti-Fe alloys resulted in the formation of a large amount of the ω phase (76–92%) [43, 45]. Also, after HPT with similar parameters (pressure 5 GPa, 1 rpm, 5–10 revolutions and pressure 6 GPa, 1 rpm, 1–10 revolutions), commercially pure titanium (CP-TI) led to the formation of 60–90% of the omega phase [50, 51]. However, it should be noted that the amount of ω-phase in commercially pure titanium pre-annealed at different temperatures formed at an HPT pressure of 6 GPa after 5 revolutions is lower than in our titanium–vanadium samples [23, 29, 64, 65]. We can assume that the increase in the portion of the ω-phase in the Ti-2 wt%V alloy with increase in pre-annealing temperature is due to two reasons. First, when the annealing temperature increases by 300 °C (from 400 to 700 °C, with an almost equal annealing time of 1992 and 1896 h, respectively), a sample annealed at a higher temperature will have larger grains and

fewer of them. As a result, in this sample, in case of HPT, a strong plastic deformation will expend less energy to overcome grain boundaries, due to which a greater amount of energy will remain in the system for phase transformations and the formation of a larger amount of ω-phase. Second, the diffusionless martensitic transition, when quenched after annealing at 1000 °C, forms a supersaturated solid solution. As a result, with the HPT, the system will spend less energy on the mass transfer necessary for the phase transformation, while more energy will remain for the transformation into the ω-phase itself. In samples annealed at 400 and 700 °C, the peaks (2; 0; 0), (1; 1; 2), (2; 0; 1), (0; 0; 4), (2; 0; 2), (1; 0; 4), (2; 0; 3) and (2; 1; 0) for the α-phase disappear after HPT. The portion of the α-phase decreases from 99% to 30 and 27%, respectively. In the sample pre-annealed at 1000 °C, not only (2; 0; 0), (1; 1; 2), (2; 0; 1), (0; 0; 4), (2; 0; 2), (1; 0; 4), (2; 0; 3), (2; 1; 0) peaks of the α-phase disappear after HPT, but also the (1; 0; 2), (2; 1; 1), (2; 1; 2) peaks and the portion of the α-phase drops from 99 to 15%. The analysis showed that most of the planes disappearing after the HPT processing belong to the pyramidal < *a* > direction {10–11} < 11–20 >. We assume that this set of planes for the α-phase most easily passes into the ω-phase. In all three samples, after HPT, the peaks of β- and ω-phases are visible. At the same time, the phase analysis did not reveal the presence of the β-phase in the samples annealed at 400 and 700 °C.

It is interesting to compare these results with the HPT influence on the α to ω transitions in binary Ti–Co and Ti–Nb alloys [13, 57]. The samples in Refs. [13, 57] were annealed, respectively, in the α-Ti + Ti₂Co and α-Ti + β-(Ti,Nb) areas of the Ti–Co and Ti–Nb phase diagrams. With increasing annealing temperature, the α-Ti-based solid solution contained more and more diluted Co. Respectively, the portion of ω-phase after HPT decreased. Moreover, in the Ti–Co the ω-phase was completely absent in the samples after HPT if they were pre-annealed just under the temperature of eutectoid decomposition of the β-phase [13, 57]. In Ref. [57], it was also observed that the smaller the amount of Nb in the α-phase, the greater the amount of the α-phase is transformed into the ω-phase.

The nanohardness of the sample pre-annealed at 400 °C varies after HPT from ≈ 4.5 ± 0.1 GPa in the center to ≈ 6.0 ± 0.1 GPa at the edges. The average value of nanohardness increases with an increase in the pre-annealing temperature from 5.1 ± 0.1 to 6.1 ± 0.1 GPa (≈ 16%). The sample annealed at 1000 °C

in the β phase area of the phase diagram is homogeneous, and the average value of its nanohardness was 6.4 ± 0.1 GPa, which is about 5% more than that of the sample annealed at 700 °C. The average nanohardness values for Ti-2.36 wt%Fe and Ti-3.93 wt% Fe alloys annealed at 470 °C and Ti-1.98 wt% Fe and Ti-2.04 wt% Fe annealed at 615 °C are $\approx 4.4 \pm 0.1$, 5.7 ± 0.1, 5.7 ± 0.1, 4.5 ± 0.2 GPa, respectively [45]. Comparison of the results leads to the conclusion that vanadium-doped titanium, after annealing and HPT processing, has higher nanohardness values than iron-doped titanium. The hardness values can be influenced by many final characteristics of the alloy; however, when comparing our results with the work [64], we see an interesting pattern that a large portion of the ω-phase corresponds to higher hardness values.

Nanohardness measurements are considered to be measurements of the surface properties of a material; therefore, to measure the volumetric properties, we additionally measured the microhardness of the samples. HPT processing has led to a significant increase in the microhardness of the materials. The resulting values correlate with the values of nanohardness (Fig. 7e). The hardness of the sample annealed at 1000 C after HPT increased from 160 to 450 HV (Fig. 7f) by almost 3 times. It can be seen that the pre-annealing temperature of the material has a real effect on its properties after HPT processing. It means that various structures formed after annealing and subsequent quenching have different effects on HPT processing. In our work, we see that the lamellar structure leads to a higher hardness than the bimodal one, consisting of lamellar and equiaxed, and consisting of martensite, lamellae and equiaxed particles leads to even slightly higher hardness than just lamellar. At the same time, the material without pre-annealing showed the highest hardness values, about 475 HV, and the same sample has the largest proportion of ωTi phase. This suggests that the dependence of HPT on pre-annealing temperature treatment is not simple.

A brief summary of all the above material: all other things being equal, different pre-annealing temperatures and HPT processing, give a different phase composition of the samples (Table 2) and a slightly different microstructure after pre-annealing at 400 °C from 700 and 1000 °C (Fig. 5). Thus, it can be concluded that these two factors are decisive for the values of micro- and nanohardness of the material. At the same time, the material without

pre-annealing (as-cast) showed the highest hardness values after HPT treatment, about 475 HV. The same sample has the largest proportion of the ωTi phase. This suggests that high microhardness values can be obtained after HPT processing if the samples are pre-annealed at 700 °C, 1000 °C and for the as-cast state.

Conclusions

(1) The pre-annealing in combination with high-pressure torsion leads to the phase transformations. As a result, the ω-phase becomes the dominant phase in Ti-2 wt%V alloy samples. With an increase in the pre-annealing temperature, its volume increases from 70 to 76%.

(2) The increase in the pre-annealing temperature leads to an increase in nanohardness values from 5.1 ± 0.1 to 6.4 ± 0.1 GPa, which is probably due to an increase in the ω-phase content in the samples. Young's module depends weaker on the pre-annealing temperature and varies from 145.5 ± 0.8 (min) to 150.6 ± 0.5 (max) GPa.

(3) The correlation between the torsion torque dependencies and those of indentation depth on the applied load were observed. The steady-state torsion torque also increases with an increase in the pre-annealing temperature, similar to the nanohardness value.

(4) The microhardness values of the samples after HPT treatment increase by about 2 times compared to annealed ones. Moreover, the higher the pre-annealing temperature, the higher the microhardness values of the material. While the microhardness of the as-cast alloy increased almost three times after the HPT, it should be noted that for the ωTi in the as-cast alloy, its amount reaches 86%. The dependences of the micro- and nanohardness of the samples on the pre-annealing temperature are consistent with each other.

Author contributions

Conceptualization was done by GSD and ASG; methodology was done by EAN and ASG; software was done by NSA, AK and AIT; validation was done by NSA, AK and AIT; formal analysis was done by AIT and EAN; investigation was done by NSA and GSD; resources were done by EAN, AK, and BBS; data curation was done by ASG and GSD; writing—original draft preparation was done by ASG and GSD; writing—review and editing was done by AIT and BBS; visualization was done by AK, AIT, and EAN; supervision was done by GSD; project administration was done by NSA and ASG; funding acquisition was done by BBS. All authors have read and agreed to the published version of the manuscript.

Funding

Data availability

All necessary data are in the text of this paper.

Declarations

Conflict of interest   No conflict of interests or competing interests exist.

References

[1]   Donachie Jr MJ (2000) Titanium: A technical guide, 2nd ed. ASM International: Materials Park, OH. 1–280

[2]   Boyer R, Collings EW, Welsch G (1994) Materials properties handbook: titanium alloys, ASM International, Materials Park, OH. 1–310

[3]   Straumal BB, Kilmametov AR, Ivanisenko Yu, Gornakova AS, Mazilkin AA, Kriegel MJ, Fabrichnaya OB, Baretzky B, Hahn H (2015) Phase transformations in Ti–Fe alloys induced by high pressure torsion. Adv Eng Mater 17:1835–1841. https://doi.org/10.1002/adem.201500143

[4]   Kutsar AR, Pavlovskii MN, Komissarov VV (1982) The observation of two-wave configuration of shock wave in titanium. JETP Lett 35:108–112

[5]   Sikka SK, Vohra YK, Chidambaram R (1982) Omega phase in materials. Prog Mater Sci 27:245–310. https://doi.org/10.1016/0079-6425(82)90002-0

[6]   Jamieson JC (1963) Crystal structures of titanium, zirconium, and hafnium at high pressures. Science 140:72–73. https://doi.org/10.1126/science.140.3562.72

[7]   Hickman BS (1969) The formation of omega phase in Ti and Zr alloys: a review. J Mater Sci 4:554–563. https://doi.org/10.1007/BF00550217

[8]   Panigrahi A, Bönisch M, Waitz T, Schafler E, Calin M, Eckert J, Skrotzki W, Zehetbauer M (2015) Phase transformations and mechanical properties of biocompatible Ti–16.1Nb processed by severe plastic deformation. J Alloys Compd 628:434–441. https://doi.org/10.1016/j.jallcom.2014.12.159

[9]   Dai N, Zhang LC, Zhang J, Zhang X, Ni Q, Chen Y, Wu M, Yang C (2016) Distinction in corrosion resistance of selective laser melted Ti-6Al-4V alloy on different planes. Corr Sci. 111:703–710. https://doi.org/10.1016/j.prostr.2020.10.092

[10]   Murray JL (1987) Phase diagrams of binary titanium alloys, 2nd ed. ASM International, Metals Park, Ohio, 1–250

[11]   Hong K-M, Shin YC (2016) Analysis of microstructure and mechanical properties change in laser welding of Ti6Al4V with a multiphysics prediction model. J Mater Proc Technol 237:420–429. https://doi.org/10.1016/j.jmatprotec.2016.06.034

[12]   Yang J, Yu H, Yin J, Gao M, Wang Z, Zeng X (2016) Formation and control of martensite in Ti-6Al-4V alloy produced by selective laser melting. Mater Design 108:308–318. https://doi.org/10.1016/j.matdes.2016.06.117

[13]   Zhao P, Fu L, Chen H (2016) Low cycle fatigue properties of linear friction welded joint of TC11 and TC17 titanium alloys. J Alloys Compd 675:248–256. https://doi.org/10.1016/j.jallcom.2016.03.113

[14]   Usikov MP, Zilbershtein VA (1973) The orientation relationship between the α- and ω-phases of titanium and zirconium. Phys Status Sol A 19:53–58. https://doi.org/10.1002/pssa.2210190103

[15]   Xia H, Parthasarathy G, Luo H, Vohra YK, Ruoff AL (1990) Crystal structures of group IVa metals at ultrahigh pressures. Phys Rev B 42:6736–6738. https://doi.org/10.1103/PhysRevB.42.6736

[16]   Zhang J, Zhao Y, Hixson RS, Gray GT III, Wang L, Wataru U, Saito H, Hattori T (2008) Experimental constraints on the phase diagram of titanium metal. J Phys Chem Sol 69:2559–2563. https://doi.org/10.1016/j.jpcs.2008.05.016

[17] Vohra YK, Sikka SK, Vaidya SN, Chidambaram R (1977) Impurity effects and reaction kinetics of the pressure-induced $\alpha \rightarrow \omega$ transformation in Ti. J Phys Chem Sol 38:1293–1296. https://doi.org/10.1016/0022-3697(77)90031-2

[18] Errandonea D, Meng Y, Somayazulu M, Häusermann D (2005) Pressure-induced $\alpha \rightarrow \omega$ transition in titanium metal: a systematic study of the effects of uniaxial stress. Physica B 355:116–125. https://doi.org/10.1016/j.physb.2004.10.030

[19] Velisavljevic N, MacLeod S, Cynn H (2012) Titanium alloys at extreme pressure conditions. In: Amin N (ed) Titanium alloys—towards achieving enhanced properties for diversified applications. InTech. 67–86. https://doi.org/10.5772/36038

[20] Trinkle DR, Hennig RG, Srinivasan SG, Hatch DM, Jones MD, Stokes HT, Albers RC, Wilkins JW (2003) New mechanism for the α to ω martensitic transformation in pure titanium. Phys Rev Lett 91:025701. https://doi.org/10.1103/PhysRevLett.91.025701

[21] Dobromyslov AV, Elkin VA (2001) Martensitic transformation and metastable β-phase in binary titanium alloys with d-metals of 4–6 periods. Scripta Mater 44:905–910. https://doi.org/10.1016/S1359-6462(00)00694-1

[22] Dobromyslov AV, Elkin VA (2006) The orthorhombic α''-phase in binary titanium-base alloys with d-metals of V-VIII groups. Mater Sci Eng A 438:324–326. https://doi.org/10.1016/j.msea.2006.02.086

[23] Edalati K, Matsubara E, Horita Z (2009) Processing pure Ti by high-pressure torsion in wide ranges of pressures and strain. Metal Mater Trans A 40:2079–2086. https://doi.org/10.1007/s11661-009-9890-5

[24] Islamgaliev RK, Kazyhanov VU, Shestakova LO, Sharafutdinov AV, Valiev RZ (2008) Microstructure and mechanical properties of titanium (grade 4) processed by high-pressure torsion. Mater Sci Eng A 493:190–194. https://doi.org/10.1016/j.msea.2007.08.084

[25] Sergueeva AV, Stolyarov VV, Valiev RZ, Mukherjee AK (2001) Advanced mechanical properties of pure titanium with ultrafine grained structure. Scripta Mater 45:747–752. https://doi.org/10.1016/S1359-6462(01)01089-2

[26] Valiev RZ, Sergueeva AV, Mukherjee AK (2003) The effect of annealing on tensile deformation behavior of nanostructured SPD titanium. Scripta Mater 49:669–674. https://doi.org/10.1016/S1359-6462(03)00395-6

[27] Todaka I, Sasaki J, Moto T, Umemoto M (2008) Bulk submicrocrystalline ω-Ti produced by high-pressure torsion straining. Scripta Mater 59:615–618. https://doi.org/10.1016/j.scriptamat.2008.05.015

[28] Todaka I, Umemoto M, Yamazaki A, Sasaki J, Tsuchiya K (2008) Effect of strain path in high-pressure torsion process on hardening in commercial purity titanium. Mater Trans 49:47–53. https://doi.org/10.2320/matertrans.ME200714

[29] Ivanisenko Y, Kilmametov A, Rösner H, Valiev RZ (2008) Evidence of $\alpha \rightarrow \omega$ phase transition in titanium after high pressure torsion. Int J Mater Res 99:36–41. https://doi.org/10.3139/146.101606

[30] Valiev RZ (2004) Nanostructuring of metals by severe plastic deformation for advanced properties. Nature Mater Res 3:511–516. https://doi.org/10.1038/nmat1180

[31] Valiev RZ, Alexandrov IV, Zhu YT, Lowe TC (2002) Paradox of strength and ductility in metals processed by severe plastic deformation. J Mater Res 17:5–8. https://doi.org/10.1557/JMR.2002.0002

[32] Edalati K, Horita Z, Mine Y (2010) High-pressure torsion of hafnium. Mater Sci Eng A 527:2136–2141. https://doi.org/10.1016/j.msea.2009.11.060

[33] Zhilyaev AP, Sabirov I, González-Doncela G, Molina-Aldareguía J, Srinivasarao B, Pérez-Prado MT (2011) Effect of Nb additions on the microstructure, thermal stability and mechanical behavior of high pressure Zr phases under ambient conditions. Mater Sci Eng A 528:3496–3505. https://doi.org/10.1016/j.msea.2011.01.062

[34] Nosova GI (1968) Phase transformations in titanium alloys, 1st ed. Metallurgy. 1–180

[35] Zwicker U (1974) Titan und titanlegierungen, 1st ed. Springer-Verlag. 1–511

[36] Ilyin AA, Kolachev BA, Polkin IS (2009) Titanium alloys, 1st ed. VILS-MATI, 520

[37] Massalski TB, Murray JL, Bennett LH, Baker H (1986) Binary alloy phase diagrams. Am Soc Metals, Metals Park, Ohio 2:2384–2386

[38] Murray JL (1981) The Ti–V (titanium-vanadium) system. Bull alloy ph diagr, Cent Mater Res 2:48–55

[39] Hu B, Sridar S, Hao L, Xiong W (2020) A new thermodynamic modeling of the Ti–V system including the metastable ω phase. Interme 122:106791. https://doi.org/10.1016/j.intermet.2020.106791

[40] Campos-Quirós A, Cubero-Sesín JM, Edalati K (2020) Synthesis of nanostructured biomaterials by high-pressure torsion: effect of niobium content on microstructure and mechanical properties of Ti-Nb alloys. Mater Sci Eng A 795:139972. https://doi.org/10.1016/j.msea.2020.139972

[41] Cvijović-Alagić I, Rakin M, Laketić S, Zagorac D (2020) Microstructural study of Ti45Nb alloy before and after HPT processing using experimental and ab initio data mining approach. Mater Charact 169:110635. https://doi.org/10.1016/j.matchar.2020.110635

[42] Edalati K, Daio T, Lee S, Horita Z, Nishizaki T, Akune T, Sasaki T (2014) High strength and superconductivity in nanostructured niobium–titanium alloy by high-pressure torsion and annealing: significance of elemental decomposition and supersaturation. Acta Mater 80:149–158. https://doi.org/10.1016/j.actamat.2014.07.065

[43] Korneva A, Straumal B, Kilmametov A, Kopacz S, Szczerba M, Cios G, Chulist R (2022) Phase transitions and mechanical behavior of Ti–3 wt% Nb alloy after high pressure torsion and low-temperature annealing. Mater Sci Eng A 857:144096. https://doi.org/10.1016/j.msea.2022.144096

[44] Deng G, Bhattacharjee T, Chong Y, Zheng R, Bai Y, Shibata A, Tsuji N (2020) Influence of Fe addition in CP titanium on phase transformation, microstructure and mechanical properties during high pressure torsion. J Alloys Compd 822:153604. https://doi.org/10.1016/j.jallcom.2019.153604

[45] Gornakova AS, Straumal BB, Mazilkin AA, Afonikova NS, Karpov MI, Novikova EA, Tyurin AI (2021) Phase composition, nanohardness and Young's modulus in Ti-Fe alloys after heat treatment and high pressure torsion. Metals 11:1657. https://doi.org/10.3390/met11101657

[46] Straumal BB, Kilmametov AR, Ivanisenko Y, Mazilkin AA, Valiev RZ, Afonikova NS, Hahn H (2018) Diffusive and displacive phase transitions in Ti–Fe and Ti–Co alloys under high pressure torsion. J Alloys Compd 735:2281–2286. https://doi.org/10.1016/j.jallcom.2017.11.317

[47] Kilmametov A, Ivanisenko Y, Straumal BB, Mazilkin AA, Gornakova AS, Kriegel MJ, Hahn H (2017) Transformations of α'martensite in Ti–Fe alloys under high pressure torsion. Scripta Mater 136:46–49. https://doi.org/10.1016/j.scriptamat.2017.04.010

[48] Janeček M, Čížek J, Stráský J, Václavová K, Hruška P, Polyakova V, Semenova I (2014) Microstructure evolution in solution treated Ti15Mo alloy processed by high pressure torsion. Mater Charact 98:233–240. https://doi.org/10.1016/j.matchar.2014.10.024

[49] Meenakshi KS, Kumar SA (2022) Corrosion resistant behaviour of titanium–Molybdenum alloy in sulphuric acid environment. Mater Today Procs 65:3282–3287. https://doi.org/10.1016/j.matpr.2022.05.389

[50] Kerber M, Waitz T, Matsuda M (2023) Structural changes of TiPt high-temperature shape memory alloys induced by high pressure torsion. J Alloys Compd 935:168037. https://doi.org/10.1016/j.jallcom.2022.168037

[51] Oliver WC, Pharr GM (1992) An improved technique for determining hardness and elastic modulus using load and displacement sensing indentation experiments. J Mater Res 7:1564–1583. https://doi.org/10.1557/JMR.1992.1564

[52] Oliver WC, Pharr GM (2004) Measurement of hardness and elastic modulus by instrumented indentation: advances in understanding and refinements to methodology. J Mater Res 19:3–20. https://doi.org/10.1557/jmr.2004.19.1.3

[53] Oliver WC, Pharr GM (2010) Nanoindentation in materials research: past, present, and future. MRS Bull 35:897–907. https://doi.org/10.1557/mrs2010.717

[54] Kilmametov A, Ivanisenko Yu, Mazilkin AA, Straumal BB, Gornakova AS, Fabrichnaya OB, Kriegel MJ, Rafaja D, Hahn H (2018) The $\alpha \rightarrow \omega$ and $\beta \rightarrow \omega$ phase transformations in Ti–Fe alloys under high-pressure torsion. Acta Mater 144:337. https://doi.org/10.1016/j.actamat.2017.10.051

[55] Korneva A, Straumal BB, Kilmametov AR, Gondek Ł, Wierzbicka-Miernik A, Lityńska-Dobrzyńska L, Chulist R, Cios G, Zięba P (2021) The $\alpha \leftrightarrow \omega$ phase transformations and thermal stability of Ti–Co alloy treated by high pressure torsion. Mater Charact 80:110937. https://doi.org/10.1016/j.matchar.2021.110937

[56] Korneva A, Straumal B, Gornakova A, Kilmametov A, Gondek Ł, Lityńska-Dobrzyńska L, Chulist R, Pomorska M, Zięba P (2022) Formation and thermal stability of ω-phase in Ti–Nb and Ti–Mo alloys subjected to HPT. Materials 15:4136. https://doi.org/10.3390/ma15124136

[57] Korneva A, Straumal B, Kilmametov A, Lityńska-Dobrzyńska L, Chulist R, Gondek Ł, Zięba P (2022) The phase transformations induced by high-pressure torsion in Ti–Nb-based alloys. Microsc Microanal 28:946. https://doi.org/10.1017/S1431927621012277

[58] Huang Y, Mortier S, Pereira PHR, Bazarnik P, Lewandowska M, Langdon TG (2017) Thermal stability and mechanical properties of HPT processed CP–Ti. In: IOP Conf. Ser.: Mater Sci Eng. 194:012012. https://doi.org/10.1088/1757-899X/194/1/012012

[59] Zayed EM, Shazly M, El-Sabbagh A, El-Mahallawy NA (2023) Deformation behavior and properties of severe plastic deformation techniques for bulk materials: a review. Heliyon 9:e16700. https://doi.org/10.1016/j.heliyon.2023.e16700

[60] Atefi S, Parsa MH, Ahmadkhaniha D, Zanella C, Jafarian HR (2022) A study on microstructure development and mechanical properties of pure copper subjected to severe plastic deformation by the ECAP-conform process. J Mater Res Technol 21:1614–1629. https://doi.org/10.1016/j.jmrt.2022.09.103

[61] Edalati K, Horita Z (2016) A review on high-pressure torsion (HPT) from 1935 to 1988. Mater Sci Eng A 652:325–352. https://doi.org/10.1016/j.msea.2015.11.074

[62] Jiang B, Men D, Emura S, Tsuchiya K (2023) Microstructural response and mechanical properties of α-precipitated Ti-5Al-5Mo-5V-3Cr alloy processed by high-pressure

torsion. J Mater Res Technol 23:564–576. https://doi.org/10.1016/j.jmrt.2023.01.047

[63] Sun K, Sun B, Yi X, Yaqian Y, Meng X, Gao Z, Cai W (2022) The microstructure and martensitic transformation of Ti-13 V-3Al light weight shape memory alloy deformed by high-pressure torsion. J Alloys Compd 895:162612. https://doi.org/10.1016/j.jallcom.2021.162612

[64] Shahmir H, Langdon TG (2016) Characteristics of the allotropic phase transformation in titanium processed by high-pressure torsion using different rotation speeds. Mater Sci Eng A 667:293–299. https://doi.org/10.1016/j.msea.2016.05.001

[65] Chen W, Xu J, Liu D, Bao J, Sabbaghianrad S, Shan D, Langdon TG (2020) Microstructural evolution and microhardness variations in pure titanium processed by high-pressure torsion. Adv Eng Mater 22:1901462. https://doi.org/10.1002/adem.201901462